DEVELOPMENT AND INVESTIGATION OF A HYBRID CURVATURE-MORPHING SKIN STRUCTURE

André Schmitz and Peter Horst

Institute of Aircraft Design and Lightweight Structures, TU Carolo-Wilhelmina Braunschweig
Hermann-Blenk-Strasse 35, D-38108 Braunschweig, Germany
Email: a.schmitz@tu-bs.de, web page: https://www.tu-braunschweig.de/ifl

Keywords: Hybrid composite, Buckling, Elastic foundation, Morphing

ABSTRACT

A short introduction on curvature-morphing skins is given. The studied structure consists of outer hybrid layers (highly strained in operation due to large curvature alterations) with unidirectional discrete composite bundles embedded in an ethylene-propylene-diene rubber foundation. Within the morphing context, the presented work focusses on the crucial aspect of compressive strength along these bundles. However, large compressive strength is achieved if buckling of the bundles can be avoided. To characterize the buckling behaviour, samples are manufactured and tested in an appropriate set-up under almost real boundary conditions (avoidance of continuous anti-buckling guides). Results are compared to the outcome of numerical linear eigenvalue analyses.

1 INTRODUCTION

Structural adaption to prevailing operating conditions has always been a topic in aerospace applications. Especially continuous contour-variable airfoil and wing morphing offers increase of performance and possibilities [1]. This work is motivated by the aerodynamic configuration of an airliner's high-lift system (particularly the droop-nose) from [2]. Recent morphing structures particularly benefit from high-performance fibre-reinforced composites, e.g. [3]. Most morphing structures can be divided into an underlying kinematic mechanism (acting as variable rib) and a skin (providing a smooth surface and taking aerodynamic load). Obviously, morphing skins must simultaneously meet counteracting requirements, namely being highly deformable in morphing-direction while providing still enough stiffness to counteract local aerodynamic pressure and loads originating from wing deflection. It turns out that most structures try to meet these conflicting specifications by imposing an extreme anisotropy: High compliance in morphing-direction is balanced by increased transverse stiffness.

However, in contrast to area-morphing, curvature-morphing skins most often need to feature a frequent change of their (bending) stiffness properties along the morphed contour [3]. Therefore, the presented skin exhibits a layered structure (Fig. 1) and can thus be manufactured with standard composite tooling, which is a strong benefit compared to other candidates like e.g. corrugated composites [4]. Here, the structural concept involves an inner FRP laminate and discrete composite bundles embedded in a compliant foundation. Presuming reasonable bond between all structural parts, the compliant foundation takes the high bending normal strain in morphing-direction, while the continuous bundles provide high transverse (bending) stiffness. Note that the direct combination of technical fibres with a compliant matrix (known as chord-rubber composites) leads to very low bending and compression strengths due to the poor buckling support of the rubber-like matrix.

The presented work experimentally focusses on the buckling behaviour along the bundles (span-wise direction). This is a crucial aspect within the sizing of the droop-nose. Ideally, the bundles show a considerably higher critical buckling strain than the failure strain of the inner laminate (cp. Fig. 1). In this case buckling failure must not be taken into account during dimensioning. Other aspects like the curvature at rupture are addressed in [5]. However, the outcome of the buckling tests is intended to validate numerical models. Precisely, the need of experimental data is motivated by the following aspects.

- The buckling problem is laying between the scales which are well described by existing theories. It is neither located at a micro-scale where one embedded fibre is completely surrounded by others, nor at a macro-scale with a single buckling column. In fact, it is an open question how an already buckled bundle influences the buckling performance of adjacent intact bundles. Additionally, there is a difference between co-operative and non co-operative buckling behaviour of adjacent bundles with respect to the initial critical strain [6]. Based on these two questions, specimens always contain multiple bundles.
- Due to the unsymmetrical boundary conditions of the foundation (bonded to the inner laminate and opposite free surface), no stand-alone test of the hybrid layer (HL) with anti-buckling guides is possible. See [7] for the impact of bonded/unbonded contact of a foundation.
- From studies of compressive failure mechanisms in standard composites [8] it is known that apart from the fibre geometry, the shear strength and the elastic behaviour of the matrix and the misalignment of the fibres mainly affect the compressive behaviour. Due to a co-curing manufacturing process (whole stacking is temporarily in a viscous phase) and a comparatively large distance between the bundles (compared to technical composites), there is increased feasibility of bundle misalignment.

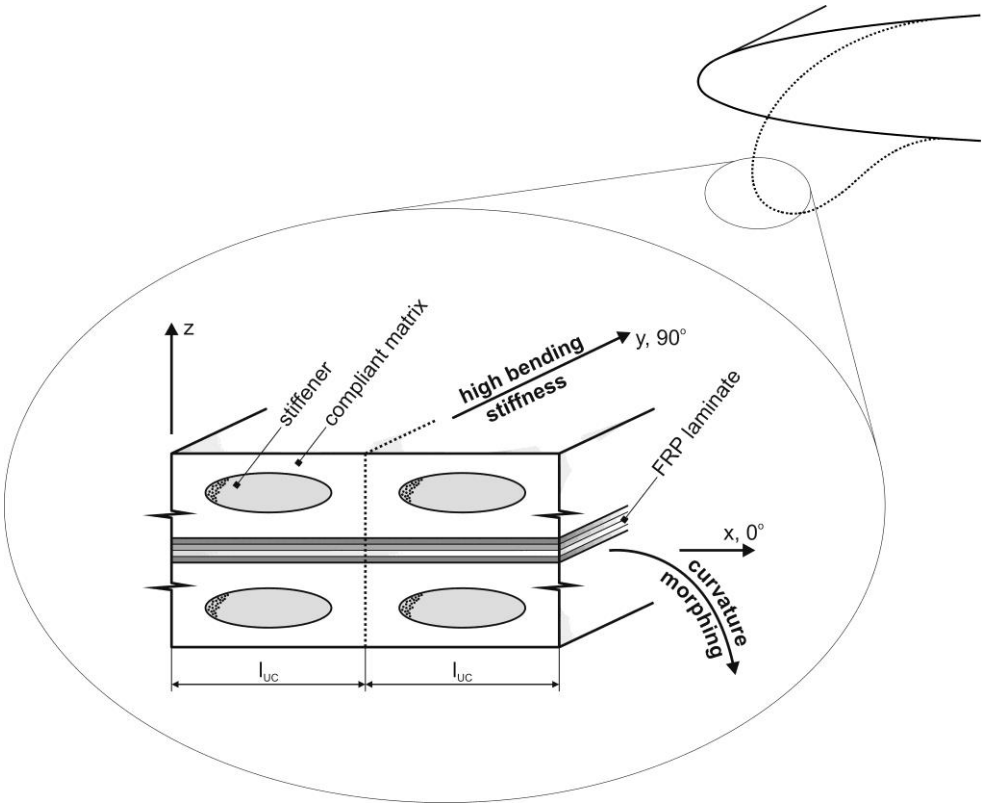

Figure 1: Sketch of the structural concept of the leading edge skin.

The following is laid out as follows. First, the dimensioning and fabrication of the specimens including constituent materials are presented. Then, the experimental set-up is described followed by the correspondent results. Finally, a summarizing conclusion is given.

2 MATERIALS AND SPECIMEN FABRICATION

The specimens are manufactured from unidirectional GFRP prepreg HexPly913® ($t_{\mathrm{ply}}^{\mathrm{GFRP}} = 0.125$ mm) for the centered laminate and the bundles and ethylene-propylene-diene rubber AA6CFZ (EPDM) for the foundation. The material data is given in Tab. 1. All bundles of the hybrid layers (HL) are cut with a specially designed cutter head ensuring equal widths and distances, see Fig.

2. Then, all constituents are ply-wisely stacked (including the rubber plies, $t_{\mathrm{ply}}^{\mathrm{EPDM}} = 0.5\,\mathrm{mm}$) and cured in a single autoclave process with $0.9\,\mathrm{bar}$ vacuum under $5\,\mathrm{bar}$ pressure at $125\,°\mathrm{C}$.

The stacking of the specimens departs from a real skin in terms of the thickness of the inner laminate, namely $[\mathrm{HL}, 0, 90_{15}, 0, \mathrm{HL}]$. The thickness of the inner laminate is a compromise. At the one hand it is exposed to the same strain as the bundles. Thus, the ratio between bundle and laminate cross-section must be large enough to clearly detect a drop of the compressive force in case of buckling of a single bundle. On the other hand the samples must be stiff enough to still withstand global Euler buckling despite already failed bundles in order to continue the experiment. At this point the influence of a failed bundle on its neighbours can then be detected. Note, that the samples become unsymmetrical throughout the experiment (in case of one-sided buckling). This in turn causes a bending moment. Although the samples are well supported (Section 3), the compliant rubber surface allows a certain bending curvature (favouring Euler buckling and precocious global failure). Hence, a strain gauge (SG) (Fig. 3 and 7) is co-cured between a HL and the inner laminate at the area of expected buckling. Hereby, the SG solder contacts are led through the surface in order to be able to cut the samples later on. Due to the shear compliant connection between the bundles with the laminate, the SG-strain is expected to equal the bundle-strain also in case of a slight sample curvature.

Finally, the samples are cut with a diamond saw and grinded to an extremely accurate rectangle oriented at the bundle direction with mean dimensions $length = 89.06\,\mathrm{mm}$, $width = 19.27\,\mathrm{mm}$ (6 bundles per width) and $thickness = 4.63\,\mathrm{mm}$.

GFRP HexPly913®			**EPDM AA6CFZ**		
E_{m}	3390	MPa	E	8.033	MPa
ν_{m}	0.380	-	ν	0.475	-
E_{f}	82800	MPa			
ν_{f}	0.230	-			
V_{f}	55.5	%			

Table 1: Material data of the constituents with subscripts $(\,)_{\mathrm{m}}$ for the epoxy matrix and $(\,)_{\mathrm{f}}$ for the E-glass fiber of the HexPly913® prepreg.

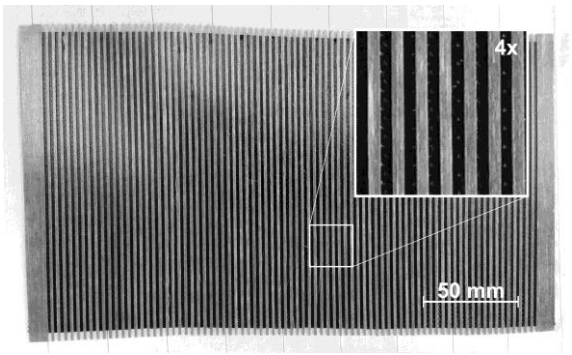

Figure 2: Stacking process step at which the cut bundles are placed above a rubber ply (black background).

3 EXPERIMENT

The aim of the experimental investigation is to analyze the buckling behavior of the embedded bundles with as real boundary conditions as possible. As discussed in Section 1, overall anti-buckling guides must hence be avoided. Figure 5 shows a sketch of the experimental set-up. Herein, the sample is prevented from global Euler buckling by supports inclined along the sample width and thus overlapping along the sample length. In contrast, each single bundle features an unsupported length which equals the distance of the top and bottom support (as the bundle width is much smaller compared to that of the whole sample).

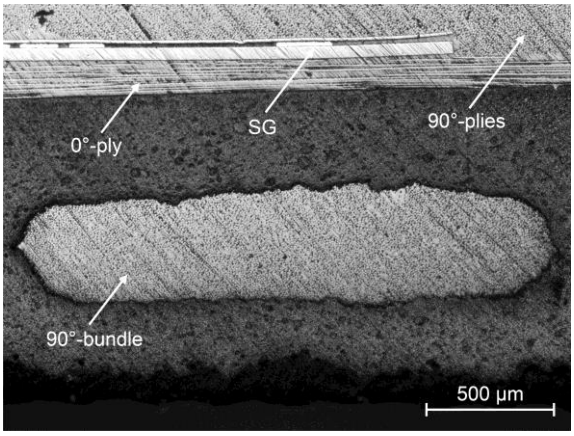

Figure 3: Microscope image of a polished section taken with a Zeiss Axio Lab.A1 (5x object lens). A complete rubber embedded bundle together with the location of the strain gauge is visible.

It is important to note, that the samples are not clamped. Even if desired it would be impossible to transfer the load through the compliant rubber surface. In fact, the supports are individually adjusted to the exact thickness (0.05 mm steps) of each sample by spacer discs. As consequence, the load is transferred only at the sample's polished top and bottom edges. The resulting constant strain throughout the whole length is advantageous:

- The compressive strain can also be detected by an inductive displacement sensor between the steel plates (cp. Fig. 4). By comparing to the SG-strain, which is measured within the free-surface section, curvature deformations are detectable.
- Except the different surface support, boundary conditions are similar for the section between and inside the supports. Hence, despite the finiteness of the free-surface buckling length, the boundary conditions meet reality as closely as possible.
- There are no undesired induced shear strains by the inclination of the supports.

Additionally, the contact surface between sample and support is equipped with a low friction Teflon film and the support inlets with a radius of $R = 0.3$ mm. Thus, the samples could be positioned between the supports by hand. Before starting the main test, the supports (Fig. 4 and 5) were traversed together up to a compression pre-force of 100 N. Hereby, the closing friction forces (32 N averaged over all samples) were relatively constant. After that, the mean distance between upper and lower support measured 9.86 mm. Hereby, the upper support is fixed to the steel plate and the bottom support is self-aligning which avoids any destructive (transverse) constraining forces. Note, that there are constrained Poisson displacements in the thickness-direction. However, since the foundation is extremely compliant compared to the centered laminate, resulting through-thickness stresses are negligible.

Finally, the steel plates are placed in the universal testing machine Zwick 1464 and closed with 1 mm/min. All data is sampled with 25 Hz in order to precisely detect buckling events.

Figure 4: Photography of the experimental set-up.

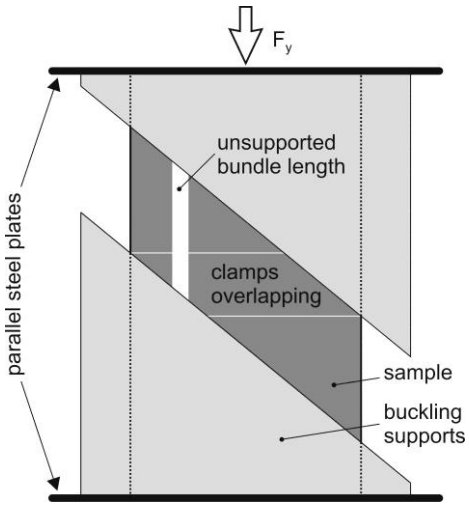

Figure 5: Sketch of the fixture.

4 RESULTS

Some insights regarding the boundary conditions (BCs) have already been gained by linear finite element eigenvalue analyses (not reported here). Namely, the buckling half-wavelength of the bundles in case of a completely free outer surface is 3.92 mm for the tested configuration. In case of the experiment boundary conditions this value slightly reduces to 3.57 mm. Accordingly, the numerical critical buckling strain rises from 1.668 % (free surface) to 1.779 % (experiment BC) of 6.7 %. However, it can be assumed that the buckling behavior is similar and thus feasible to investigate as representative configuration.

Figure 6 presents the summary of the experimental results. Herein, the SG-strain is plotted against the compressive load per sample width for 3 samples. All buckling events are indicated by a circle. The hybrid plies always contain 6 bundles per sample width. Originating from the manufacturing process, the mean cross-section of the bundles of the opposite HLs slightly differs (4.8 %). This means, that a certain initial asymmetry exists. Additionally, the buckling strain of the smaller bundles is little lower, too. For this reason, buckling could only be observed at the HL with the smaller bundles (at the side of the co-cured strain gauges). Note, that the asymmetry of a sample rises with each buckled bundle making buckling at the opposite HL more and more unlikely due to a slight curvature of the sample. Figure 7 shows the free-surface section of one specimen after testing. As expected, the buckling locations follow the inclination of the supports. Obviously, bundle buckling leads to irreversible damage. Final failure is indicated by the end of the load/strain curves in Fig. 6 and always originate from the high surface pressure by breakage of the sample's top or bottom faces.

From 15 microscope images (like Fig. 3) the exact geometries are measured directly with the microscope und used as input for the above mentioned linear eigenvalue analysis. The critical strain turns out to be 1.779 ± 0.094 % (assuming a Gaussian distribution). With this result the experimental outcome of 1.513 ± 0.308 % can be interpreted. It seems that almost one third of the standard deviation is already due to the inherent different geometries of the bundles. From Fig. 6 the suspicion seems approved that a buckled bundle can influence neighbouring bundles in terms of precocious failure of the latter resulting in lower experimental buckling strains. Additionally, there will be imperfections and misalignments compared to the numerical model. However, buckling events never occur at the same strain (cp. Fig. 6). Thus, any co-operative behaviour as mentioned in [6] can be excluded. With these considerations it can be concluded that the numerical and experimental results match well.

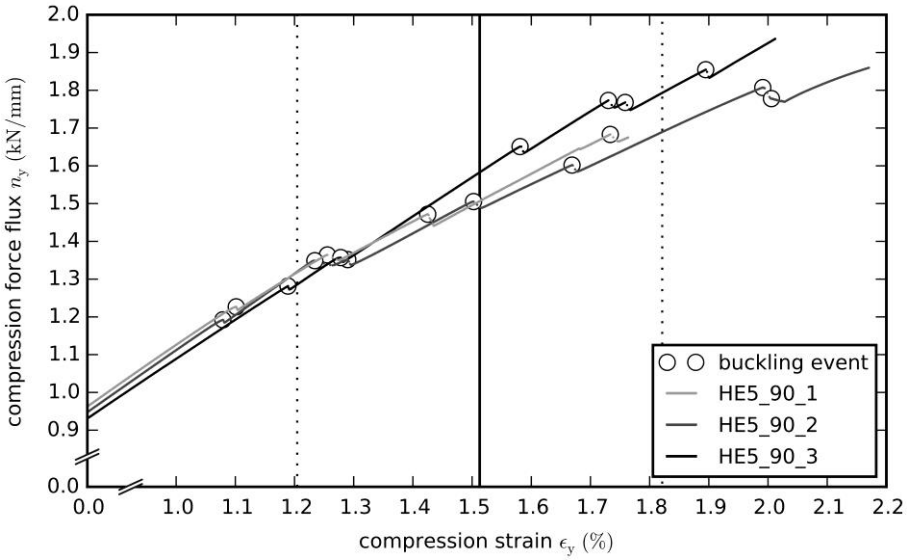

Figure 6: Strain gauge compressive strain against line load of 3 samples. Buckling of a bundle is indicated by a circle. The end of the load/strain curves represents final failure. The experimental mean buckling strain with Gaussian standard deviation (17 events) of 1.513 ± 0.308 % is plotted.

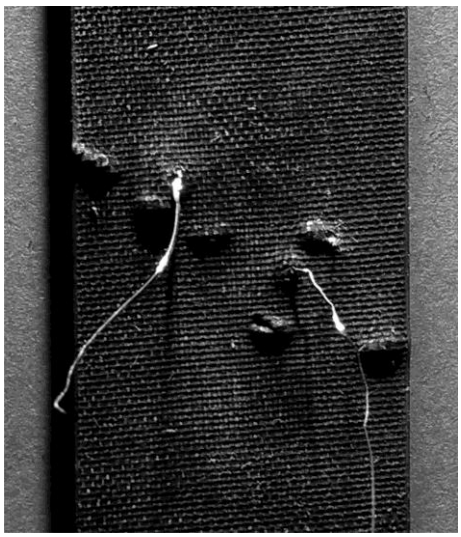

Figure 7: Photography of the section between the supports of a sample after testing. All 6 bundles of the hybrid layer have been irreversibly buckled.

4 CONCLUSIONS

The presented work deals with an important aspect within the development of a curvature-morphing skin structure. Precisely, the buckling behavior of discrete composite bundles embedded in a compliant rubber foundation is investigated. Due to the scale of the bundles with respect to the skin structure and the distinct boundary conditions, a special specimen design and experimental set-up is used. Results from linear eigenvalue finite element analyses are shortly reported and match the experimental outcome. Beside the validation of the theory, the combined effect of bundle misalignment and impact of buckled bundles on intact neighbors could be quantified. Any co-operative buckling behavior could be excluded.

ACKNOWLEDGEMENTS

Funding for this work is provided by the German Research Fundation DFG through the collaborative research center (SFB) 880 ”Fundamentals of high-lift for Future Civil Aircraft”.

REFERENCES

[1] S. Barbarino, O. Bilgen, R.M. Ajaj, M.I. Friswell and D.J. Inman, A review of morphing aircraft, *Journal of Intelligent Material Systems and Structures*, **22**, 2011, pp. 823-877.

[2] M. Burnazzi and R. Radespiel, Design and analysis of a droop nose for Coanda flap applications, *Journal of Aircraft*, **51(5)**, 2014, pp. 1567-1579.

[3] M. Kintscher, M. Wiedemann, H.P. Monner, O. Heintze and T. Kühn, Design of a smart leading edge device for low speed wind tunnel tests in the European project SADE, *International Journal of Structural Integrity*, **2**, 2001, pp. 383-405.

[4] A. Schmitz and P. Horst, Bending deformation limits of corrugated unidirectionally reinforced composites, *Composite Structures*, **107**, 2014, pp. 103-111.

[5] A. Schmitz and P. Horst, A new curvature morphing skin: Manufacturing, experimental and numerical investigations, *Proceedings of the 16th European Conference on Composite Materials, Seville, Spain*, 2014.

[6] C. Müller, A. Gorius, S. Nazarenko, A. Hiltner and E. Bär, Co-operative microbuckling of two fibres in a model composite, *Journal of Materials Science*, **31**, 1996, pp. 2747-2755.

[7] K.S. Papachristou and D.S. Sophianopoulos, Buckling of beams on elastic foundation considering discontinuous (unbonded) contact, *International Journal of Mechanics and Applications*, **3(1)**, 2013, pp. 4-12.

[8] P.M. Jelf and N.A. Fleck, Compression failure mechanisms in unidirectional composites, *Journal of Composite Materials*, **26**, 1992, pp. 2706-2726.